Tuning the Compact Linear Collider 380 GeV final-focus system using realistic beam-beam signals

J. Ögren, A. Latina, R. Tomás, and D. Schulte
European Organization for Nuclear Research (CERN), Geneva, Switzerland

(Received 18 February 2020; accepted 11 May 2020; published 27 May 2020)

Tuning of the final-focus system of a linear e^-e^+ collider is a challenging problem due to the strong nonlinearities of the system and small transverse beam sizes at the interaction point. To have reliable performance of a collider, nominal luminosity must be reached quickly under a set of various imperfections. Measuring luminosity at high energies is a nontrivial task, and, to get a precise measurement, many collisions must be sampled. Therefore, it is desirable to use other beam-beam signals for faster tuning. This paper studies the use of beamstrahlung and incoherent pairs in an extensive simulation study including static imperfections. Tuning results of the nominal lattice are compared to an updated lattice with a smaller vertical beam size at the interaction point. Finally, recovery time after machine downtime and misalignment of components due to ground motion is also studied.

DOI: 10.1103/PhysRevAccelBeams.23.051002

I. INTRODUCTION

The Compact Linear Collider (CLIC) [1–3] is a proposed linear electron-positron collider at CERN. To reach the nominal luminosity of 1.5×10^{34} cm^{-2} s^{-1}, CLIC relies on nanometer beam sizes at the interaction point (IP). This puts tight constraints on emittance preservation along the whole machine, and imperfections causing emittance growth must be mitigated. CLIC is foreseen to be built in three energy stages ranging from 380 GeV to 3 TeV. In this report, we limit our discussion to the first energy stage. The nominal beam parameters for the CLIC 380 GeV energy stage are summarized in Table I. The emittances at the end of the main linac assume that all the upstream sections (ring-to-main-linac transfer and main linac) use all of their emittance budgets. Hence, since it is likely that the emittance growth from the upstream sections is smaller than that, this scenario is somewhat pessimistic.

A. The CLIC final-focus system

The CLIC final-focus system constitutes the final 780 m of the electron and positron main beam lines. The system is mirror symmetric with respect to the IP and has the purpose to collimate, transport, demagnify, and finally bring into collision the electron and positron beams. Luminosity, which is a measure of the number of collisions, serves as a quality measure for a linear collider and can be expressed [4] as

$$\mathcal{L} = H_D \frac{N^2}{\sigma_x \sigma_y} n_b f_{\mathrm{rep}} \tag{1}$$

where N is the number of particles per bunch, n_b is the number of bunches per pulse, and f_{rep} is the repetition rate. These parameters are all machine specific. The transverse beam sizes at the IP, σ_x and σ_y, and the correction factor H_D, which include effects from the "hourglass" effect and disruption enhancement (two beams with opposite charge focus each other), are, on the other hand, determined by the final-focus system.

The beam size at the IP is constrained by the optics, in particular, the beta functions at the IP and the beam emittances, according to

$$\sigma^*_{x,y} = \sqrt{\beta^*_{x,y} \varepsilon_{x,y}}, \tag{2}$$

where small beta functions are achieved by the strong quadrupole magnets in the final doublet. The current nominal lattice has $L^* = 6$ m, which allows the final quadrupoles to be mounted fully outside the detector volume [5,6]. To compensate for the chromatic effects (particles with different energy are focused differently), bending magnets to generate dispersion and sextupole magnets for position-dependent focusing are both needed. The CLIC final-focus system follows a local chromaticity-correction scheme [7], with sextupoles interleaved, and chromaticity corrected locally, close to the final doublet. Additional sextupoles are placed upstream in the final-focus system, and phase advances

TABLE I. CLIC 380 GeV beam parameters.

Parameter	Unit	Value
Norm. emittance (end of linac) $\gamma\epsilon_x/\gamma\epsilon_y$	[nm]	900/20
Norm. emittance (IP) $\gamma\epsilon_x/\gamma\epsilon_y$	[nm]	950/30
Beta function (IP) β_x^*/β_y^*	[mm]	8.2/0.1
Target IP beam size σ_x^*/σ_y^*	[nm]	149/2.9
Bunch length σ_z	[μm]	70
rms energy spread δ_p	[%]	0.35
Bunch population N_e	[10^9]	5.2
Number of bunches n_b		352
Repetition rate f_{rep}	[Hz]	50
Luminosity $\mathcal{L}_{\mathrm{total}}$	[10^{34} cm^{-2} s^{-1}]	1.5
Peak luminosity $\mathcal{L}_{1\%}$	[10^{34} cm^{-2} s^{-1}]	0.9

between the sextupoles are such that many of the unwanted geometric aberrations cancel. Figure 1 shows the optical functions and dispersion profile for the nominal CLIC 380 GeV final-focus system. The system contains 20 quadrupole magnets, six sextupole magnets, and two octupole magnets for tail folding. The nominal final-focus system has $\beta_y^* = 100$ μm, but recent efforts [8] have been made for a low-β_y^* lattice, the same overall layout but with the optics redesigned to achieve $\beta_y^* = 70$ μm instead.

B. Previous tuning studies

Tuning is about achieving nominal performance for an imperfect system. For instance, static imperfections such as magnet misalignments will alter the optics, since off-centered quadrupoles generate extra dispersion and off-centered sextupoles generate additional focusing. This may lead to a waist shift at the IP or imperfect cancelation of geometric aberrations due to changes in phase advances between sextupoles. Since the final-focus system is highly nonlinear, small imperfections can have dramatic consequences on the luminosity.

Tuning for CLIC has been studied extensively, and significant progress has been made over the years. The tuning of the CLIC 3 TeV final-focus system under static imperfections was studied in Refs. [9–11] and including dynamic imperfections in Ref. [12]. An updated tuning study of the CLIC 380 GeV nominal final-focus system was presented in Ref. [13]. That study showed substantial improvement in the tuning time. However, that study also considered a simplified case: one-beam tuning, where only half of the system was simulated and the beam at the IP was mirrored for the beam-beam simulations.

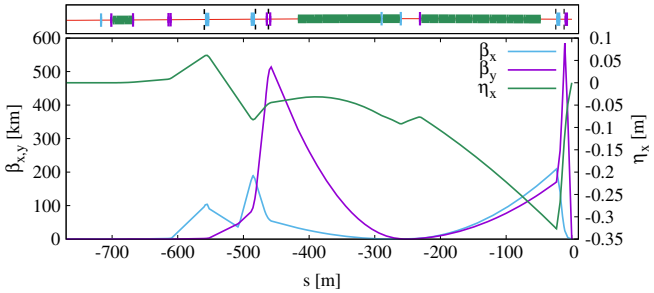

FIG. 1. Beta functions and dispersion function for the nominal $L^* = 6$ m CLIC 380 GeV final-focus system.

C. Two-beam tuning with realistic signals

In this paper, we consider two-beam tuning where the electron and positron beam lines are treated independently with individual static imperfections. We use the particle tracking code PLACET [14] for tracking the beams through the magnetic lattice, and all simulations include effects from synchrotron radiation. To evaluate the luminosity and compute other beam-beam signals, we perform full beam-beam simulations using the code GUINEA-PIG [15].

The aim of the tuning simulation is to achieve high luminosity, and in previous studies the luminosity signal has been used as a tuning signal. However, luminosity can be difficult and time consuming to measure precisely at high energies, especially in the beginning of the tuning procedure, where the luminosity is low. Then, it is more realistic to rely on other signals, and in this study we make use of beamstrahlung and incoherent pair production instead. These two signals are explained in the next section.

II. BEAM-BEAM SIGNALS

The beam-beam effect in a linear collider is quite extreme and quite different from the beam-beam effect in a circular collider. The very small beam sizes at interaction in a linear collider cause high disruption—particles have significant motion during collision—due to the concentrated charge and intense electromagnetic fields of the opposing bunch. Since particles travel on bent trajectories, they can emit synchrotron radiation, and, in the context of the beam-beam effect, this is referred to as beamstrahlung. More information on the beam-beam effect in linear colliders can be found in Ref. [16].

A. Beamstrahlung

The scaling laws for beamstrahlung [17] in the classical regime can be simplified and written as

$$n_\gamma \propto \frac{N}{\sigma_x + \sigma_y}, \tag{3}$$

$$E_\gamma \propto \frac{N}{(\sigma_x + \sigma_y)\sigma_z}, \tag{4}$$

where we note that both the number of photons and the average photon energy are inversely proportional to the sum of transverse beam sizes at the IP. It follows that the average power of emitted beamstrahlung is inversely proportional to the square of the sum of the transverse beam

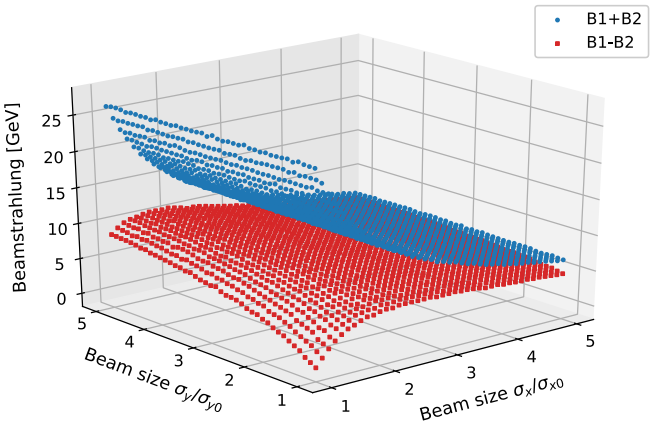

FIG. 2. Simulation of the emitted beamstrahlung during a head-on collision between a nominal beam (beam 2) and a nominal beam with scaled transverse beam sizes (beam 1). The total beamstrahlung (B1 + B2) has a strong dependence on the horizontal beam size. From beamstrahlung asymmetry (B1 − B2), we can also determine which is the larger beam.

sizes. Beamstrahlung is undesired, since particles lose energy before collision. This is also the reason there are two targets in Table I, one for total luminosity and one for the luminosity within the 1% energy peak. To minimize beamstrahlung for a given luminosity, it is advantageous to collide flat beams, i.e., to have one transverse dimension small and one large. In CLIC, the horizontal beam size is much larger than the vertical. This is a logical choice, since the damping rings naturally provide beams with a much smaller vertical emittance than horizontal.

In a simulation study, we investigated the emitted beamstrahlung power and its dependence on the transverse beam size. By simulating a perfect final-focus system, we obtained a nominal beam distribution. We then ran multiple beam-beam simulations for a nominal beam colliding with a beam with scaled transverse dimensions. Figure 2 shows the sum and difference of the average photon energy emitted by the two beams for different relative transverse beam sizes. There is a clear horizontal beam size dependence on the total energy (sum signal) but little dependence on the vertical beam size, and this is explained by the fact that the beam is 50 times larger horizontally than vertically. This is true in the case where we have a nominal beam and a nominal beam with a scaled transverse beam size as in Fig. 2, but there can be situations where the beams are far away from nominal sizes, and then this is no longer true. From the difference signal—beamstrahlung asymmetry—it is possible to determine which beams is the largest. To first order, we will use total beamstrahlung as a horizontal beam size indicator. The main beam and the beamstrahlung photons will travel through the same beam pipe after collision. Dipole magnets before the beam dump will displace the main beam such that beamstrahlung photons and beam particles enter the beam dump at different locations. In this way, the total deposited energy from beamstrahlung can be measured.

B. Incoherent pairs

In the collisions, electron-positron pairs can be generated via a process called incoherent pair production. This is a two-particle interaction where either real photons (from beamstrahlung) or virtual photons interact. There is also a process called coherent pair production, where a beamstrahlung photon interacts with the macroscopic electromagnetic fields from the opposing beam. Coherent pairs are created only for high-energy particles and intense electromagnetic fields. For CLIC 380 GeV, the coherent pairs are a negligible signal but not for the CLIC 3 TeV energy stage.

Naturally, the probability of incoherent pair production increases with increasing luminosity. In the CLIC detector, there is a dedicated system for detecting incoherent pairs called the BeamCal [6] with the purpose of providing luminosity estimates to aid the tuning. The BeamCal is an electromagnetic calorimeter installed on both sides, about 3 m from the IP, in the very forward region as shown in Fig. 3. Incoherent pair production is simulated in GUINEA-PIG, and, to achieve the distribution of incoherent pairs, the produced particles are also tracked through the electromagnetic fields of the opposing beam. To determine the deposited energy in the BeamCal, we transform into coordinates of transverse momentum and polar angle and cut for particles with correct angles and sufficient momentum not to be deflected by the detector solenoid field. Figure 4 shows the distribution of created incoherent pairs in the forward direction of the electron beam during a nominal collision. The figure also displays the cut of particles ending up in the BeamCal.

To assess the relationship between incoherent pairs and luminosity, we launched a simulation study of a perfect machine but with sextupoles misaligned. For each case, we ran the beam-beam simulation 10 times. Figure 5 displays the luminosity and total incoherent pair energy deposited in

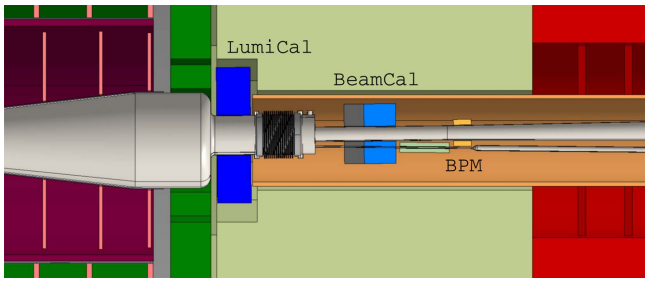

FIG. 3. The forward region of the CLIC detector. The interaction point is to the left, and the spent beam and the beamstrahlung photons leave the detector through the outgoing beam pipe. The LumiCal is a dedicated detector for precise luminosity measurements from Bhabha events, whereas the purpose of the BeamCal is to provide a quick luminosity estimation by measuring incoherent electron-positron pairs.

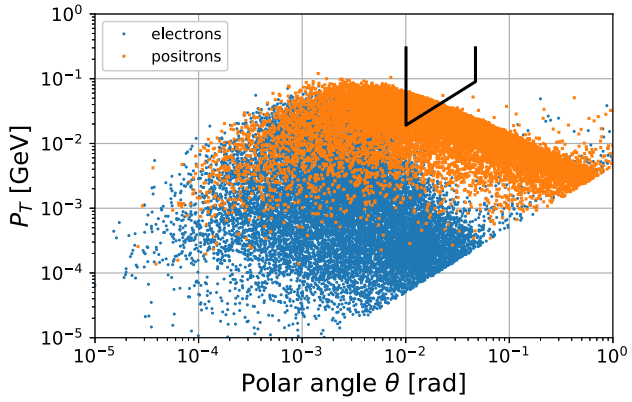

FIG. 4. The distribution of electrons and positrons emitted in the forward direction of the electron main beam. Particles with the correct angles, and sufficient energy not to be deflected by the 4 T detector magnetic field, will end up in the BeamCal (marked with black lines). Positrons will be deflected by the opposing positron main beam, and, hence, more positrons than electrons end up in the BeamCal; the converse is true for the incoherent pairs emitted in the forward direction of the positron main beam.

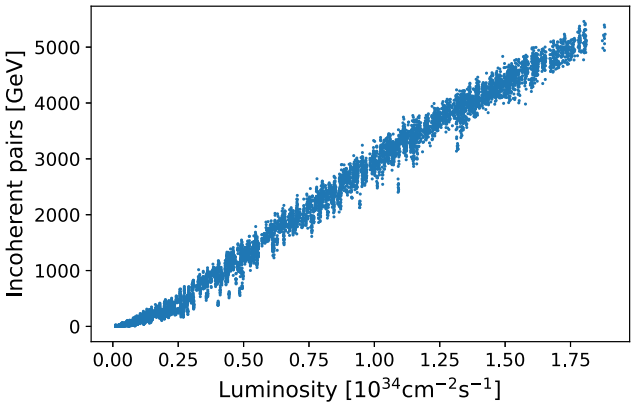

FIG. 5. Simulation of 1000 cases with randomly distributed sextupole offsets. For each case, the full beam-beam simulation was run 10 times. We plot the luminosity and total energy in incoherent pairs in the BeamCal.

the BeamCal. Above a certain threshold, there is a clear linear correlation between the two signals. However, the signal from the incoherent pairs is significantly more noisy than the luminosity. This is mainly due to statistical fluctuations due to the low counting rate of the incoherent pairs. In our tuning, we seek to maximize luminosity by maximizing the deposited energy in the BeamCal from incoherent pairs. To deal with the noise, we make a single parabolic fit to a large number of points, and, if the range is sufficient, this is a robust strategy. Figure 6 shows an example of a scan of a sextupole linear knob where the best knob gain is found from the maximum of the parabola. In the simulation, we consider single-bunch collisions, but, if

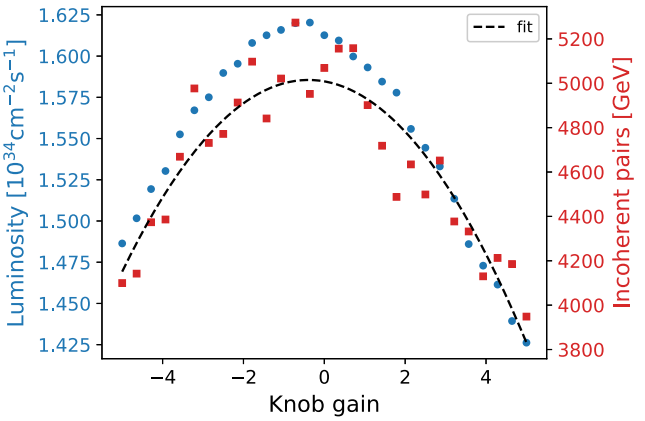

FIG. 6. An example of a sextupole linear knob scan. We plot the luminosity signal together with the incoherent pairs signal. A single parabolic fit provides a robust method of finding the optimum, provided that we scan over a sufficient range and use a large number of points.

we average over 352 bunches in a train, the noise should be reduced by a factor of $\sqrt{352} \approx 19$.

III. TUNING PROCEDURE

In this section, we outline the tuning procedure used in this study. The first step is beam-based alignment, where the linear optics is corrected by moving the quadrupoles transversely. The majority of the following steps are optimization of the nonlinear optics with sextupole tuning, including a random walk optimizer and tuning with sextupole knobs. Finally, we use a method where the linear and the nonlinear optics are simultaneously corrected in a combined quadrupole and sextupole random walk optimization.

A. Beam-based alignment

In beam-based alignment, the beam position monitors (BPMs) are used to measure the position of the beam, and the beam trajectory is, in our case, controlled by transverse movement of the quadrupoles. To straighten the trajectory, the beam is centered in every BPM. However, the BPMs might have transverse offsets, and, if the beam is off center in the quadrupoles, additional dipole kicks will induce extra dispersion that can have a negative impact on the chromatic correction. Therefore, we also measure and correct dispersion.

For the beam-based alignment, we use an all-to-all approach [18]. The linear optics can be modeled as the linear system

$$\begin{bmatrix} \vec{x}_{\mathrm{BPM}} \\ w\vec{\eta} \end{bmatrix} = \begin{bmatrix} R_x \\ wR_\eta \end{bmatrix} \vec{x}_{\mathrm{quad}}, \tag{5}$$

where $\vec{x}_{\mathrm{BPM}}$ denotes the horizontal and vertical beam positions, $\vec{\eta}$ the horizontal and vertical dispersion, and

$\vec{x}_{\mathrm{quad}}$ the horizontal and vertical position of the quadrupoles. The dispersion is measured by comparing the trajectory of two beams with different energies; for CLIC, a relative energy difference of 0.1% is used. Response matrices R_x and R_η can be measured by moving individual quadrupoles and measuring the change in beam position and dispersion. The weight w is introduced, since the uncertainty in the measurement of the beam position might be different than the uncertainty in the dispersion measurement.

First, the response matrices are measured on the imperfect machine, and the measured trajectory and dispersion are compared to target values. The linear system above is inverted to find quadrupole positions to move the trajectory and dispersion toward target values. The matrix is typically ill conditioned, but it can be inverted using singular-value decomposition and removing the smallest eigenvalues before inversion [19]. The response matrices are measured once, but the correction is done iteratively, and we use about 30 iterations. Throughout the beam-based alignment, sextupole and octupole magnets were switched off to avoid influence from the nonlinear magnetic fields. In the beam-based alignment, the electron and positron beam lines are corrected independently and could be done in parallel.

B. Sextupole tuning

Sextupole transverse misalignments in the final-focus system have a high impact on the luminosity. Therefore, it is crucial to have robust methods for correcting the sextupole transverse position. For each side of the final-focus system, there are six sextupoles, each mounted on movers with the possibility of horizontal and vertical movement.

1. Sextupole alignment

In the previous one-beam tuning study presented in Ref. [13], a new sextupole alignment method was used, where sextupoles were powered and aligned one by one. This method showed excellent robustness and could bring the machine to a good state, in some cases even reaching the target luminosity. However, investigations showed that using the same procedure in the two-beam scenario with realistic signals is problematic. In the beginning of the alignment, when only one or two sextupoles are powered and luminosity is around 10^{30}–10^{31} $\mathrm{cm}^{-2}\,\mathrm{s}^{-1}$, beam sizes are too large to give a usable signal from the incoherent pairs, and with beamstrahlung we have effectively only a signal for the horizontal beam size. Therefore, we do not use this alignment method but instead use a random walk optimization with all sextupoles powered on.

2. Random walk optimizer

With six sextupoles and two transverse directions, we have 12 degrees of freedom, and we look for directions in this space that result in minimizing the beam size at the IP. We do not select a random direction in the full 12-dimensional space, but instead we randomly select a subset and then scan a random direction in this subspace. We use the following steps for the random walk algorithm: (1) Select a random subset of six out of the 12 degrees of freedom. (2) Select a random direction. (3) Scan 7 steps along this direction. (4) Make a parabolic fit and find the maximum of the signal. (5) Go to the optimum position. (6) Go back to step 1 and iterate until the threshold is reached. Naturally, there is a trade-off between scanning many points along each direction in order to accurately determine the optimum position and sampling many directions, since not all directions have an impact on the signal.

In the tuning, we use two versions of this algorithm. First, to maximize the total beamstrahlung power—this will mainly tune the horizontal beam size. After this step, the luminosity is high enough to give a signal in the incoherent pairs. The next step is the same random walk algorithm to maximize the incoherent pairs. Since the horizontal beam size is already tuned, an increase in the incoherent pairs signal will mainly be due to a decrease in the vertical beam size.

3. Sextupole linear knobs

When a machine is in a state with luminosity close to the target, systematic scans of sextupole knobs can be a more efficient way of reaching the target compared to a random walk procedure. A knob [20,21] is a linear combination of settings that has a certain effect on the machine. Ideally, knobs are orthogonal, such that an individual parameter can be changed while others remain unchanged. We construct linear sextupole knobs from multiparticle tracking simulations. A response matrix is computed with each column corresponding to the change in second-order moments of the beam distribution at the IP due to the movement of a single sextupole. We denote the second-order moments as σ_{ij} with $i, j \in \{x, x', y, y', \delta, z\}$ and the horizontal position of sextupole k as X_k and obtain

$$R_X = \begin{bmatrix} \frac{\partial \sigma_{xx}}{\partial X_1} & \cdots & \frac{\partial \sigma_{xx}}{\partial X_6} \\ \frac{\partial \sigma_{xx'}}{\partial X_1} & \cdots & \frac{\partial \sigma_{xx'}}{\partial X_6} \\ \vdots & \cdots & \vdots \\ \frac{\partial \sigma_{zz}}{\partial X_1} & \cdots & \frac{\partial \sigma_{zz}}{\partial X_6} \end{bmatrix} \tag{6}$$

and similarly R_Y for vertical sextupole movements. There are 21 unique second-order moments, and, thus, R_X is a 21×6 matrix. The knobs can be constructed by using singular-value decomposition on the response matrices, and for the horizontal case we have $U\lambda V^T = R_X$. We use columns of matrix V as our knobs, and these are orthogonal by construction. Thus, our sextupole knobs are collective movements of the sextupoles, in the horizontal and vertical

directions, that have an orthogonal impact on the beam distribution at the IP.

C. Combined quadrupole and sextupole tuning

The complex interplay between the linear and nonlinear optics is one of the reasons tuning of the final-focus system is challenging. After beam-based alignment, the linear optics is set and quadrupole settings are not changed. Sextupole transverse offsets can compensate many effects due to the additional focusing. However, in some cases, the sextupole tuning cannot reach the target luminosity. One question arises: What if the linear optics was not corrected well enough? Any movement of quadrupoles after sextupole tuning will result only in a decrease in luminosity, since the sextupoles were tuned to optimize luminosity given the current state of the linear optics. The solution is to move quadrupoles and sextupoles together.

We use a random walk optimization similar to what was presented in the previous section. In this case, we have 52 degrees of freedom (20 quadrupoles, six sextupoles, and two transverse directions), and again we randomly select a subset and then a random direction. For each direction, a seven-point scan is performed, and then the setting that maximizes the signal from incoherent pairs is selected.

D. The full procedure

The first step is correcting the linear optics by performing beam-based alignment of the two beam lines; this can be done simultaneously. This is followed by sextupole tuning, first random walk optimizers and then systematic scanning of the sextupole knobs. Experience has taught us that the linear sextupole knobs are effective for tuning when the state of the machine is not so far from the ideal working point, within about 10% of the nominal luminosity or above. This is not so surprising, considering that the sextupole linear knobs are designed with a linear approximation for a perfect machine; as the imperfect machine is far away from the perfect state, the knobs are not orthogonal. This is the reason we first use a random walk optimizer to bring the imperfect machine to a state where the linear sextupole knobs can be effective. The full tuning procedure consists of: (1) Beam-based alignment (BBA). (2) Sextupole random walk maximizing beamstrahlung power. (3) Sextupole random walk maximizing incoherent pairs signal. (4) Multiple iterations of sextupole linear knobs maximizing incoherent pairs signal. (5) Quadrupole and sextupole random walk (if the target is not reached) maximizing incoherent pairs signal. (6) Multiple iterations of sextupole linear knobs (if the target is not reached) maximizing incoherent pairs signal.

The beam-based alignment can be done in parallel for the electron and positron beam lines. Random walk tuning is done one beam line at the time. From beamstrahlung asymmetry, it can be inferred which of the two beams is larger. However, this does not always work, and, in the early stage of the tuning when beam sizes are far from nominal, there are scenarios where this does not work. Instead, we randomly select which beam line to tune. For the tuning knobs, again one beam line is tuned at a time. Typically, we scan knob 1 in the electron beam line followed by knob 1 in the positron beam line and so on.

IV. TUNING SIMULATIONS

To assess the effectiveness of the tuning procedure, we subject a set of 500 machines to randomly distributed static imperfections. The tuning goal is that a minimum of 90% of the machines should achieve 110% of nominal luminosity, where the extra 10% is added as a luminosity budget for dynamic imperfections. If 90% of the machines are tuned successfully, given the tolerances, it is a high probability that the actual machine could be successfully tuned. For the cases that cannot be successfully tuned, some intervention with realignment of the beam line would be required.

A. Simulation setup

For each of the 500 machines, we added individual, randomly distributed imperfections to the electron and positron beam lines using the tolerances from Table II as rms values. The tolerances listed are the specified tolerances for CLIC [1] but with the alignment tolerance for the multipoles relaxed from 10 to 20 μm. For the beam-based alignment, we used two single-particle beams with 0.1% energy difference for measuring dispersion. We consider the resolution, roll errors, and transverse misalignments as imperfections of the BPMs. Additional uncertainties, not included in this study, are scale factor errors of the BPMs and uncertainty in the energy difference of the two beams for dispersion measurements.

For the tuning, we used a beam of 20 000 macroparticles for the early stages of the tuning and a beam of 100 000 macroparticles for the later stages where fine-tuning is required. Between each tuning stage, the luminosity was evaluated using a 100 000-macroparticle beam. Similar to Ref. [13], we used a beam from an integrated simulation in order to have a beam with a realistic correlation between the longitudinal position and energy.

B. Results

Figure 7 shows the luminosities after the different steps of the tuning procedure, where each line is sorted for

TABLE II. Tolerances used as rms values for the applied static imperfections in the final-focus system.

Imperfection	Tolerance	Element
Resolution	20 nm	BPMs
Transverse misalignments	10 μm	BPMs and magnets
Transverse misalignments	20 μm	Multipole magnets
Roll errors	100 μrad	BPMs and magnets
Relative strength errors	10^{-4}	Magnets

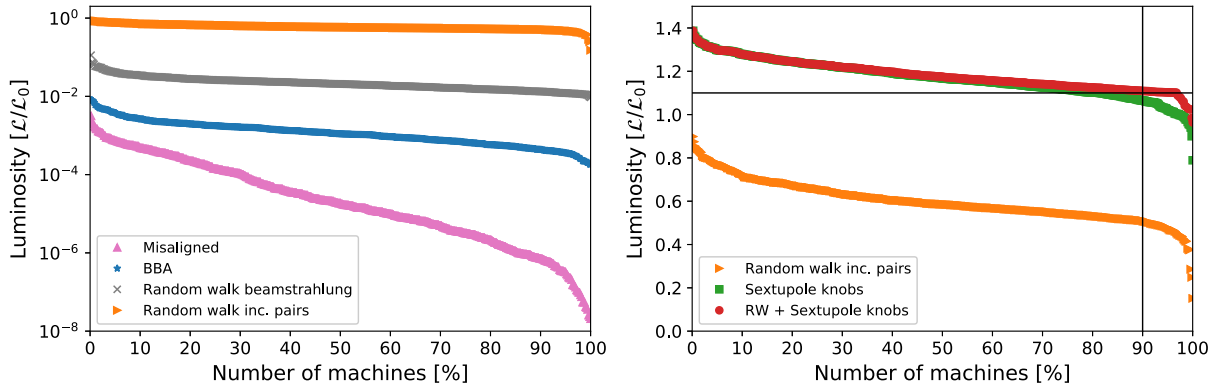

FIG. 7. Luminosity histogram after different steps of the tuning process. Left: The early steps of the tuning process. At the starting point, luminosity is ranging almost down to 8 orders of magnitude from the nominal values. Right: The final stages of the tuning (linear scale y axis). The straight lines mark the tuning goal: 90% of the machines should reach the target of 110% of nominal luminosity.

readability. We note that before any tuning, when all static imperfections are added, the luminosity ranges from 3 to 8 orders of magnitude below the nominal luminosity. After beam-based alignment, luminosities range from 2 to 4 orders of magnitude below the target. The sextupole random walk methods manage to bring almost all machines above 40% of the nominal luminosity. Around 80% of the machines exceeded the luminosity target after tuning with the sextupole knobs. For the machines that did not reach the target, we applied the combined quadrupole and sextupole random walk tuning followed by additional tuning with the sextupole knobs. In the end, 96.8% of the machines reached the luminosity target, thus exceeding the goal of 90%. The worst case reached 96% of nominal luminosity and, thus, within 87% of the target. The tuning results are summarized in Table III.

It is interesting to note that the quadrupole and sextupole combined random walk tuning in some cases did not improve the luminosity directly. Instead, luminosity stayed on a similar level, but the state of the machine was different, which is the reason that the sextupole knob tuning that followed could still improve the luminosity. The combined quadrupole and sextupole random walk allows a change of the state of the machine while keeping luminosity on a similar level. This was the key to the high success rate in this tuning study.

TABLE III. Results of the tuning studies of the nominal and the low-β_y^* lattices.

	Nominal	Low β_y^*
Vertical beta function at IP [μm]	100	70
Number of machines	500	500
Target luminosity [$\mathcal{L}_{\text{target}}/\mathcal{L}_0$]	1.1	1.1
Maximum luminosity [$\mathcal{L}_{\text{max}}/\mathcal{L}_0$]	1.39	1.41
Minimum luminosity [$\mathcal{L}_{\text{min}}/\mathcal{L}_0$]	0.96	0.97
Mean luminosity [$\mathcal{L}_{\text{mean}}/\mathcal{L}_0$]	1.18	1.21
Median luminosity [$\mathcal{L}_{\text{median}}/\mathcal{L}_0$]	1.17	1.21
Number of machines reaching target	96.8%	94.6%
Maximum number of measurements	7601	6392
Minimum number of measurements	630	686
Mean number of measurements	2370	2081
Median number of measurements	2104	1900

For machine performance, the tuning time is an important parameter. One wants to reach high luminosity quickly. Figure 8 shows a histogram of the tuning time (after the beam-based alignment) expressed as the number of measurements. In the simulation, a measurement is a collision of two bunches. In the real machine, a measurement would be a collision of two bunch trains (352 bunches per train) with a repetition rate of 50 Hz.

The best case machine tuned in 630 measurements, and 90% of the machines reached the luminosity target in 4100 measurements or less. The worst case needed 7601 measurements to reach the luminosity target, and the median machine required 2104 measurements to tune—this should be compared to the 900 measurements needed in the one-beam study [13]. However, keep in mind that in this study we have the added complexity of two independent beam lines. Furthermore, we changed to a more realistic sextupole alignment procedure and used more realistic signals from beamstrahlung and incoherent pair production. CLIC would operate with a repetition rate of 50 Hz, so, in principle, 2100 measurements can be achieved in less than a minute. In reality, there are other effects to consider, such as the time needed for settings to be applied and magnets to move, and at each knob setting a few shots should be recorded to average out additional noise. Furthermore, we have assumed an ideal IP feedback and head-on collisions for each measurement, but in reality a few shots might be required for the feedback to ensure a head-on collision after changing a knob setting. Nonetheless, we stress that the number of measurements needed by the tuning procedure puts a lower limit on the tuning time and that quick tuning is essential for machine availability.

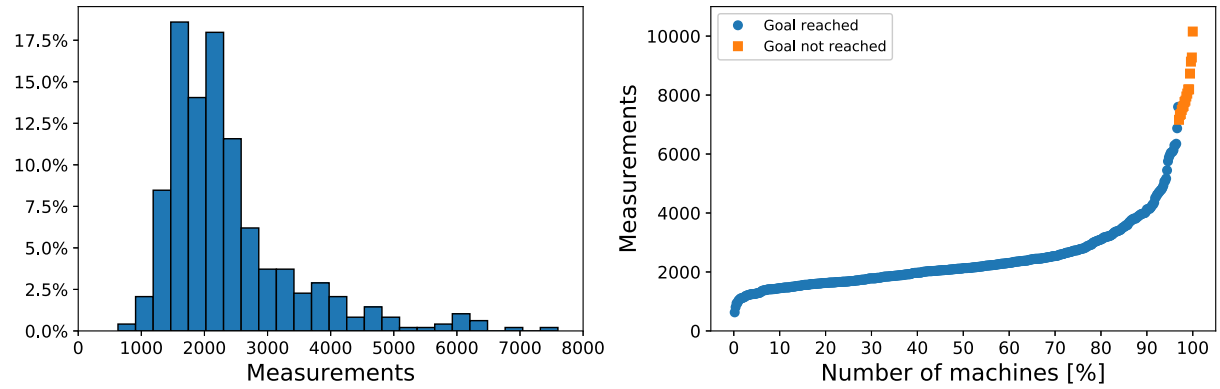

FIG. 8. Left: Histogram of the total number of measurements needed to reach the target luminosity. The median of the number of measurements is 2104. Right: Cumulative distribution of number of measurements needed to reach the luminosity target. 90% of machines reached the target in 4100 measurements or less.

C. Luminosity evolution

Figure 9 shows the luminosity evolution of the median machine (after beam-based alignment was applied) with the number of measurements on the horizontal axis. We plot the transverse beam sizes for the two beams, the tuning signals—beamstrahlung and incoherent pairs—and, finally, the luminosity. The luminosity is plotted only for reference and was not used by any of the tuning algorithms. In the simulation, we use single-bunched beams for computational reasons, but the values for beamstrahlung and luminosity in the figure are both scaled with the number of bunches per bunch train and repetition rate.

Starting with sextupole random walk tuning and maximizing beamstrahlung power, we observe a clear decrease in the horizontal beam size of the two beams. The sextupole random walk with maximization of incoherent pairs started after 147 measurements when the threshold was reached, and during this tuning step there is a slow but steady

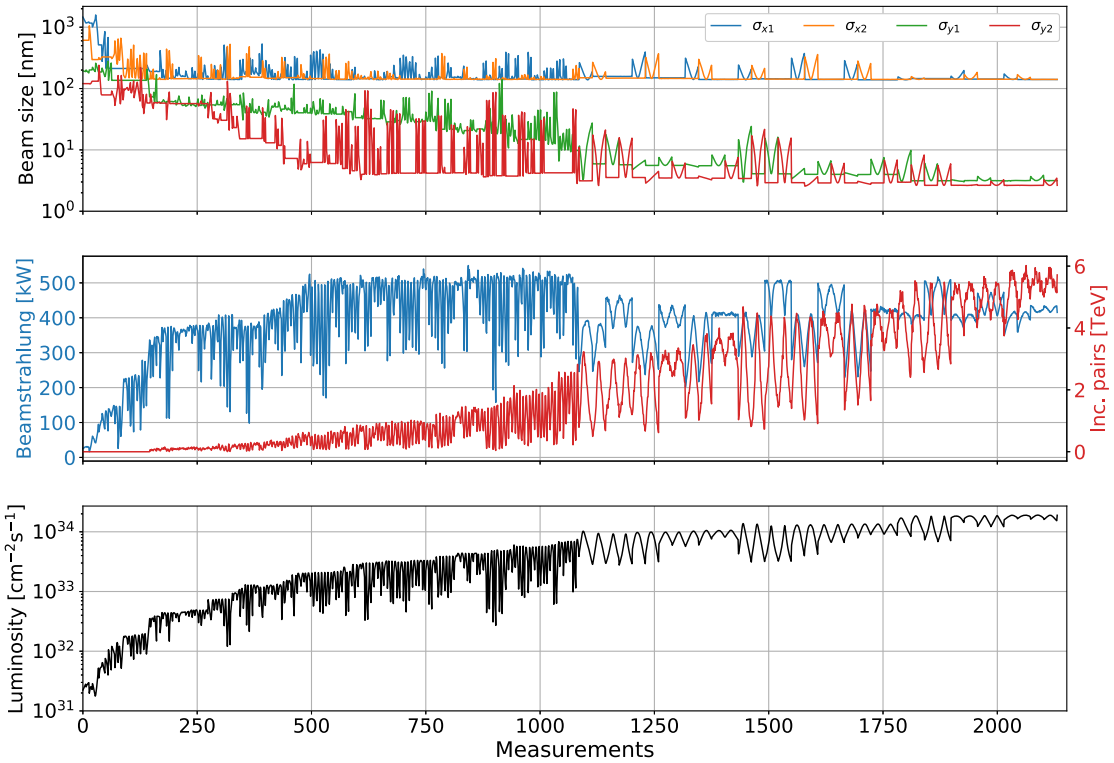

FIG. 9. The luminosity tuning evolution of the median machine after beam-based alignment has been performed. The horizontal axis display the number of measurements. Top: The horizontal and vertical beam sizes of the two beams. Middle: The two tuning signals. Bottom: The luminosity—this signal is only for reference and was not used in the tuning simulation.

increase in the incoherent pairs signal due to a decrease in the vertical beam size. After 1086 measurements, the sextupole knob scans start, and there is a clear change in character: a more systematic scan, where the first knob is scanned for the electron beam line followed by the same for the positron beam line and so on. We also note that the luminosity is quite high after around 1100 measurements, and this could already be useful physics production. From an operational point of view, the fine-tuning could be done slowly such that the machine is carefully brought from 80% of nominal luminosity to 100% while taking data. In this study, we aimed at reaching the target as quickly as possible, but the number of measurements needed to reach a state of useful luminosity is lower than the number of measurements to reach the target.

D. Tuning the low-β_y^* lattice

In the low-β_y^* lattice, the optics was redesigned to decrease the vertical beam size at the IP. Studies showed that decreasing β_y^* from 100 to 70 μm resulted in a 4.5% increase in luminosity for a perfect machine [8]. To investigate if this new optics impacts the tuning performance, we performed an identical simulation study for this lattice. Again, we submitted a set of 500 machines to randomly distributed imperfections and tuned with the same methods. The results for both the nominal and the low-β_y^* lattices are summarized in Table III.

For a sample size of 500 machines, the differences observed in Table III between the two lattices are not statistically significant. The luminosity for the low β_y^* is slightly higher, but, on the other hand, the success rate was slightly lower yet well above the target. We conclude that, from a tuning perspective, the two lattices show comparable performance. Figure 10 compares the histograms of the number of measurements needed to reach the luminosity target. It is not surprising that the low β_y^* tunes somewhat faster, since the increased nominal luminosity gives some additional overhead. Again, the difference is small, and we conclude that the tuning performance does not seem to be affected by the change in β_y^*, and, since the low β_y^* has increased luminosity by design, this is the preferred choice.

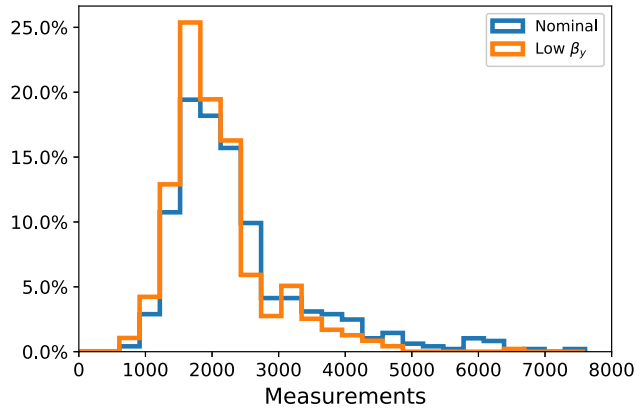

FIG. 10. Histograms of the total number of measurements needed to reach the target luminosity for the nominal lattice and the low-β_y lattice. The average tuning time was slightly lower for the low-β_y lattice.

V. LUMINOSITY RECOVERY

In this paper, we have studied the impact of static imperfections. Fast tuning is important not just for machine performance and luminosity production, but also for dealing with dynamic imperfections. In this section, we investigate the impact of ground motion. The scenario studied is the following: If the machine goes down for a certain time, ground motion will slightly misalign the accelerator components and without the possibility to apply beam-based correction. How long does it take to recover the luminosity after the machine has been down for a certain time? Here, we take the median machine from the nominal lattice tuning study and misalign the components using the ATL-law [22] ground motion generator in PLACET using $A = 0.5 \times 10^{-6}$ μm^2 s^{-1} m^{-1}. This corresponds to "model B" in Ref. [1]. We do not continuously apply ground motion; instead, we treat it as a static imperfection.

To recover luminosity, two methods are applied. First, we apply one-to-one steering on both beam lines to recover the previous trajectories, which we assumed were stored. Then we do two quick scans of the sextupole knobs, again using the incoherent pairs as a signal. The required number of shots per beam line for the one-to-one steering is about 120, and this could be done for the two beam lines in parallel. One iteration of the sextupole knobs scan uses about 90 measurements.

Figure 11 shows the luminosity recovery for downtimes up to 1 and 24 h. The time on the horizontal axis denotes the downtime. The first line shows the luminosity after the machine has been misaligned from ground motion and then luminosity after one-to-one steering and two iterations of sextupole knob scans. After 30 min of downtime, the luminosity is reduced to about 70% of the luminosity at time 0 and one-to-one steering brings the machine back to only 90% of luminosity before downtime. For the first 24 h, one-to-one steering followed by a single iteration of sextupole knobs scan is sufficient to recover luminosity. Figure 12 shows luminosity recovery for downtimes up to 7 days. As we can see, one-to-one steering followed by two quick scans of the sextupole knobs manages to recover luminosity fairly well even for long downtimes.

This simplified study shows that luminosity can be recovered quickly after downtimes as long as 24 h when components have been misaligned due to ground motion. For longer downtimes, the quick procedure does manage to quickly bring the luminosity back to 80%–90% of the initial luminosity. Naturally, there are additional effects not included here, and during a longer downtime the state of the

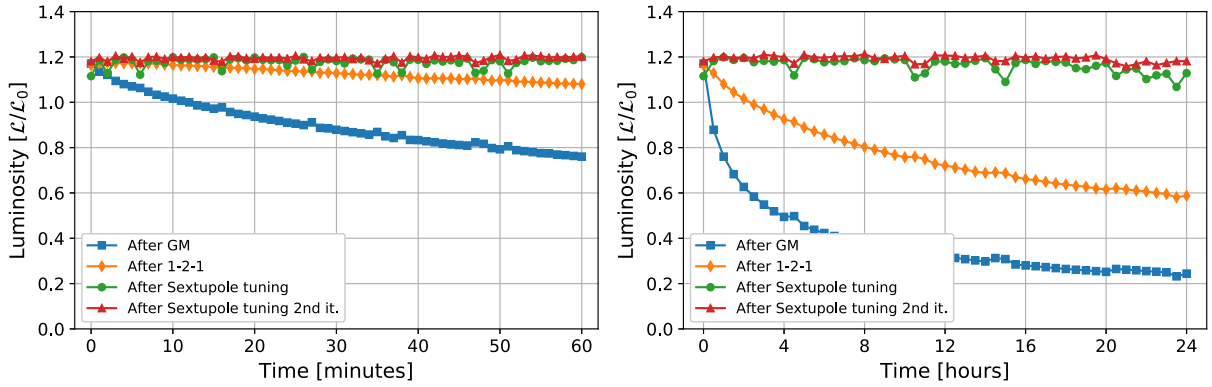

FIG. 11. Left: Luminosity recovery after downtimes up to 60 min. Right: Luminosity recovery for downtimes up to 24 h. We plot the luminosity for the machine misaligned by ground motion, the luminosity after one-to-one steering, and the luminosity after the first and second iterations of scanning the sextupole knobs.

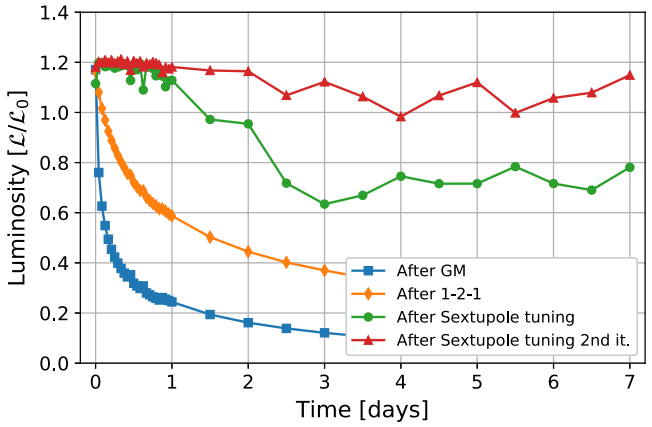

FIG. 12. Luminosity recovery for downtimes up to 7 days.

machine might be different. At least it is clear that the component misalignment due to ground motion does not pose a big challenge. The state of the machine after misalignments due to ground motion is much better than the initial state in the tuning study in previous sections. For instance, there was no need to perform a full beam-based alignment, random walk optimization of the sextupoles, etc., since the one-to-one steering puts the machine back in a good state where the sextupole knobs can efficiently tune the luminosity back to optimum.

VI. FUTURE OUTLOOKS

The list of imperfections considered in this study is not exhaustive. For instance, the impact of various dynamic imperfections such as beam jitter and energy jitter, crab cavity imperfections, and detector solenoid imperfections has not been considered. In this study, we also assumed an idealized IP feedback, which brings the beams into collision instantaneously. The influence on tuning time of a realistic IP feedback should also be the topic of future studies. BPM scale factor errors, additional magnetic multipole errors, and mover tolerances for magnets are also topics of future studies.

VII. CONCLUSIONS

Achieving high luminosity under imperfect conditions is crucial for the reliability of a collider. The final-focus system, in particular, is crucial and especially challenging due to its nonlinearities. In this paper, we considered static imperfections and utilized beam-beam signals such as beamstrahlung and incoherent pairs as probes for guiding the tuning. This approach seems more practical than direct measurements of luminosity, since precise luminosity measurements are expected to be time consuming and not viable in the early stage of tuning when luminosity might be very low. The study showed substantial improvements on both robustness and tuning time for the tuning of the final-focus system. These are important steps toward showing the feasibility of successfully operating a high-luminosity linear collider.

In a simulation study of 500 machines, the final-focus system was subjected to randomly distributed static imperfections. The tuning procedure includes beam-based alignment, sextupole random walk optimization, tuning with sextupole knobs, and, finally, a combined quadrupole and sextupole random walk optimization. After the full tuning procedure, 96.8% of the machines successfully reached the luminosity target, and, thus, we exceeded the goal of 90% of machines to tune successfully. The median machine required 2104 measurements to reach the target, and 90% of machines reached the target in 4100 measurements or less. The same tuning procedure was applied to a redesigned, low-β_y^* version of the final-focus system with comparable success rates and tuning times.

The effect of misalignments due to ground motion during machine downtime was also studied. One-to-one steering was applied to restore the previous beam trajectory, followed by two quick scans of the sextupole knobs.

For downtimes up to 24 h, one-to-one steering and a single scan of the sextupole knobs were sufficient to recover the luminosity. This procedure required only around 120 shots for beam-based alignment followed by 90 measurements of sextupole tuning. Thus, misalignments due to ground motion during machine downtime should have a small impact on luminosity performance.

[1] A multi-TeV linear collider based on CLIC technology: CLIC conceptual design report, edited by M. Aicheler, P. Burrows, M. Draper, T. Garvey, P. Lebrun, K. Peach, N. Phinney, H. Schmickler, D. Schulte, and N. Toge, CERN Report No. CERN-2012-007.

[2] Updated baseline for a staged Compact Linear Collider, edited by P. N. Burrows, P. Lebrun, L. Linssen, D. Schulte, E. Sicking, S. Stapnes, and M. A. Thomson, CERN Report No. CERN-2016-004, CERN, Geneva, 2016.

[3] The Compact Linear Collider (CLIC)—Project implementation plan, edited by M. Aicheler, P. N. Burrows, N. Catalan, R. Corsini, M. Draper, J. Osborne, D. Schulte, S. Stapnes, and M. J. Stuart, CERN Report No. CERN-2018-010-M.

[4] J.-P. Delahaye, G. Guignard, T. Raubenheimer, and I. Wilson, Scaling laws for e^+/e^- linear colliders, Nucl. Instrum. Methods Phys. Res., Sect. A **421**, 369 (1999).

[5] F. Plassard, A. Latina, E. Marin, R. Tomás, and P. Bambade, Quadrupole-free detector optics design for the Compact Linear Collider final focus system at 3 TeV, Phys. Rev. Accel. Beams **21**, 011002 (2018).

[6] CLICdp Collaboration, The post-CDR CLIC detector model, CERN Report No. CLICdp-Note-2017-001, 2017.

[7] P. Raimondi and A. Seryi, Novel Final Focus Design for Future Linear Colliders, Phys. Rev. Lett. **86**, 3779 (2001).

[8] A. Pastushenko, New CLIC FFS design at 380 GeV, in *Proceedings of the CLIC Workshop 2019, CERN, Geneva* (to be published).

[9] B. Dalena, J. Barranco, A. Latina, E. Marin, J. Pfingstner, D. Schulte, J. Snuverink, R. Tomas, and G. Zamudio, Beam delivery system tuning and luminosity monitoring in the Compact Linear Collider, Phys. Rev. Accel. Beams **15**, 051006 (2012).

[10] E. Marin, A. Latina, R. Tomás, and D. Schulte, Final focus system tuning studies towards Compact Linear Collider feasibility, Phys. Rev. Accel. Beams **21**, 011003 (2018).

[11] F. Plassard, Optics optimization of longer L^* beam delivery system designs for CLIC and tuning of the ATF2 final focus system at ultra-low β^* using octupoles, Ph.D. thesis, CERN-THESIS-2018-223, 2018.

[12] E. Marin, A. Latina, D. Schulte, R. Tomás, and J. Pfingstner, Tuning of CLIC-final focus system 3 TeV baseline design under static and dynamic imperfections, J. Phys. Conf. Ser. **1067**, 022014 (2018).

[13] J. Ögren, A. Latina, D. Schulte, and R. Tomás, Tuning of the CLIC 380 GeV final-focus system with static imperfections, CERN Report No. CERN-ACC-2018-0055, 2018.

[14] The tracking code PLACET, https://clicsw.web.cern.ch/clicsw/.

[15] D. Schulte, Study of electromagnetic and hadronic background in the interaction region of the TESLA collider, Ph.D. thesis, DESY-TESLA-97-08, TESLA-97-08, Germany, 1996.

[16] D. Schulte, Beam-beam effects in linear colliders, CERN, Geneva Report No. CERN-2017-006-SP 2017.

[17] A. W. Chao and M. Tigner, *Handbook of Accelerator Physics and Engineering* (World Scientific, Singapore, 1999), Sec. II.6.

[18] A. Latina and P. Raimondi, A novel alignment procedure for the final focus of future linear colliders, in *Proceedings of the 25th International Linear Accelerator Conference, LINAC-2010, Tsukuba, Japan, 2010* (KEK, Tsukuba, Japan, 2010).

[19] W. H. Press, S. A. Teukolsky, W. T. Vetterling, and B. P. Flannery, *Numerical Recipes in C*, 2nd ed. (Cambridge University Press, Cambridge, England, 1992).

[20] Y. Nosochkov, P. Raimondi, T. Raubenheimer, and A. Seryi, Tuning knobs for the NLC final focus, SLAC Report No. SLAC-PUB-9255, 2002.

[21] T. Okugi *et al.*, Linear and second order optics corrections for the KEK Accelerator Test Facility final focus beam line, Phys. Rev. Accel. Beams **17**, 023501 (2014).

[22] A. Seryi and O. Napoly, Influence of ground motion on the time evolution of beams in linear colliders, Phys. Rev. E **53**, 5323 (1996).